nature structural & molecular biology

Protein refolding is required for assembly of the type three secretion needle

Ömer Poyraz[1,5,6], Holger Schmidt[2,6], Karsten Seidel[2,5,6], Friedmar Delissen[3], Christian Ader[2,5], Hezi Tenenboim[1], Christian Goosmann[4], Britta Laube[4], Andreas F Thünemann[3], Arturo Zychlinsky[1], Marc Baldus[2,5], Adam Lange[2], Christian Griesinger[2] & Michael Kolbe[1]

Pathogenic Gram-negative bacteria use a type three secretion system (TTSS) to deliver virulence factors into host cells. Although the order in which proteins incorporate into the growing TTSS is well described, the underlying assembly mechanisms are still unclear. Here we show that the TTSS needle protomer refolds spontaneously to extend the needle from the distal end. We developed a functional mutant of the needle protomer from *Shigella flexneri* and *Salmonella typhimurium* to study its assembly *in vitro*. We show that the protomer partially refolds from α-helix into β-strand conformation to form the TTSS needle. Reconstitution experiments show that needle growth does not require ATP. Thus, like the structurally related flagellar systems, the needle elongates by subunit polymerization at the distal end but requires protomer refolding. Our studies provide a starting point to understand the molecular assembly mechanisms and the structure of the TTSS at atomic level.

Shigella dysentery, typhoid fever and the plague are diseases that affect more than 20 million people per year. Understanding the disease mechanism could open the door to inexpensive treatments for these diseases, which affect mainly developing countries. The bacterial species that cause these life-threatening diseases require a TTSS to deliver virulence factors. TTSSs consist of a multiannular base crossing both bacterial membranes and an extracellular needle-shaped structure[1–9]. The major needle component—YscF, PrgI and MxiH in *Yersinia enterocolitica*, *S. typhimurium* and *S. flexneri*, respectively—is a small protein (protomer) that is conserved among TTSSs[10] (**Supplementary Fig. 1**). Recent studies in *Y. enterocolitica*[2] and *S. typhimurium*[11] elegantly show that TTSS proteins that interact with the protomer control the length of the growing needle. However, the protomer could not be investigated in detail due to its spontaneous polymerization. To advance our understanding of this huge macromolecular system, it is essential to analyze its assembly mechanism. Here we address the questions of how the soluble cytosolic protomers switch into a polymerization-competent state and to which end of the needle these proteins are attached during growth[12–15].

RESULTS

Design of a functional and soluble needle protomer mutant

Thus far, biophysical and biochemical studies of TTSS needles have used C-terminally truncated protomers that were soluble but nonfunctional. In a systematic mutagenesis screen, we identified a mutant that is soluble when expressed heterologously in *Escherichia coli* (**Fig. 1a**). This mutant carries modifications in two conserved residues near the C terminus (Val65 and Val67, referring to the PrgI sequence from *S. typhimurium* in **Supplementary Fig. 1**). Notably, this V65A V67A double mutant (*prgI**) is fully functional, as it complements a *prgI* knockout in *S. typhimurium* (Δ*prgI*) as efficiently as wild-type *prgI* in secretion (data not shown) and epithelial cell invasion assays (**Fig. 1b**).

Polymerization of purified TTSS needle protomer mutants

Notably, purified PrgI* and its homolog MxiH* from *S. flexneri* spontaneously polymerize, forming a gel at high concentrations (**Supplementary Fig. 2**). PrgI* assembles into nonamyloid filaments, as shown by weak enhancement of thioflavin T fluorescence[16] during polymerization and X-ray fiber diffraction experiments[17] of *in vitro* needles lacking the 4.7-Å peak that is typical for cross–β-structures (**Supplementary Fig. 3**). Transmission electron microscopy (TEM) revealed that needle protomers form defined spicular structures (**Fig. 1c** and **Supplementary Fig. 4**) 10–13 nm in diameter. This diameter corresponds to that of TTSS needles of *S. typhimurium* analyzed by cryo–electron microscopy[8,18], supporting the functionality of protomer mutants. Purified PrgI* or MxiH* polymerize into very long needles (several μm in length instead of 50–70 nm for native needles; **Fig. 1c** and **Supplementary Fig. 4**) similar to reconstituted TTSS needles from *Pseudomonas aeruginosa*[19]. In agreement with recent reports *in vivo*, these results suggest that the needle length may be controlled by specific proteins, such as PrgJ[8] and InvJ[20] in *S. typhimurium* or YscP in *Y. enterocolitica*[11].

[1]Max-Planck-Institute for Infection Biology, Cellular Microbiology, Berlin, Germany. [2]Max-Planck-Institute for Biophysical Chemistry, NMR based Structural Biology, Göttingen, Germany. [3]BAM Federal Institute for Material Research and Testing, Berlin, Germany. [4]Max-Planck-Institute for Infection Biology, Core Facility Microscopy, Berlin, Germany. [5]Present addresses: BASF SE, Ludwigshafen, Germany (K.S.), Bijvoet Center for Biomolecular Research, Utrecht University, Utrecht, The Netherlands (C.A. and M.B.) and Department of Medical Biochemistry and Biophysics, Karolinska Institutet, Stockholm, Sweden (Ö.P.). [6]These authors contributed equally to this work. Correspondence should be addressed to A.L. (adla@nmr.mpibpc.mpg.de) or M.K. (kolbe@mpiib-berlin.mpg.de).

Received 8 November 2009; accepted 1 April 2010; published online 13 June 2010; doi:10.1038/nsmb.1822

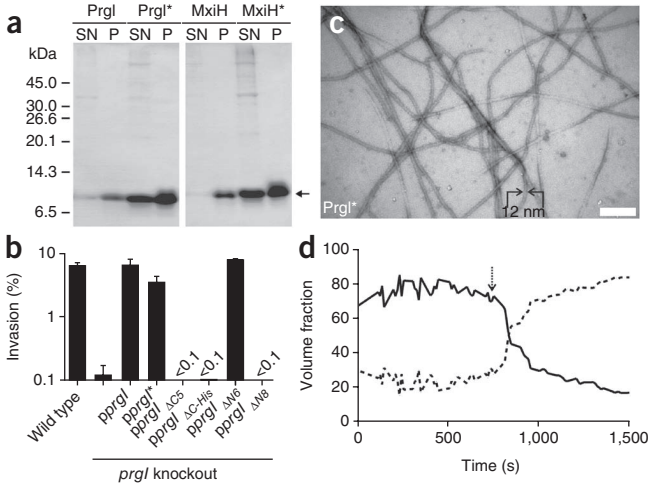

Figure 1 Polymerization of a functional TTSS protomer. (**a**) SDS-PAGE of PrgI, PrgI*, MxiH and MxiH* expressed in *E. coli*. Double mutants were detected in soluble (SN) and insoluble (P) fractions, whereas wild-type protomer was almost insoluble (arrow). (**b**) Epithelial cell invasion assay showed wild type activity of *S. typhimurium* protomer knockouts complemented with either wild-type gene (p*prgI*) or protomer mutant (p*prgI**). Percent bacterial invasion is logarithmically scaled. Deletion (p*prgI* ΔC5) or fusion (p*prgI* ΔC-His) of residues at the PrgI C terminus, as well as deletion of the N-terminal eight residues (p*prgI* ΔN8), abolished cell invasion. (**c**) TEM image of negatively stained needles formed *in vitro* by purified PrgI* (scale bar, 200 nm). (**d**) Time-dependent monomer conversion of PrgI* (solid line) versus needle growth (dashed line) monitored by DLS. Arrow, end of the lag phase.

The assembly of TTSS needles *in vitro* can be divided in two steps, nucleation and elongation[21]. We analyzed the kinetics of PrgI* polymerization to determine the rate-limiting step using dynamic light scattering (DLS). With this method, we measured the volume fractions of the monomer and the growing needle. In this process, a lag phase was followed by needle growth in conjunction with a rapid decrease in free protomer concentration (**Fig. 1d**). The kinetic behavior indicates that nucleation is the rate-limiting step in PrgI* needle formation and might be indicative of the behavior of the wild-type protein.

Elongation of the TTSS needle *in vitro*

It is not known whether, during *in vivo* TTSS assembly, the newly synthesized protomers are transported through the growing needle to the distal end or are incorporated at the proximal end[22]. To test this, we mixed isolated TTSSs from either *S. typhimurium* or *S. flexneri* (see Online Methods) with purified protomer PrgI* or MxiH*, respectively. Addition of the autologous protomer elongated TTSS needles substantially (**Fig. 2a**,**b**), to more than 5 µm in average length (**Fig. 2c**). TTSSs without protomer addition showed particles of constant length only (**Fig. 2c**). These results show the structural compatibility of the mutated and autologous protomers. We observed that the assembly is directional, as each elongated needle emerged from a single TTSS (**Fig. 2b**, enlarged images). Notably, we did not observe needle elongation after the addition of the heterologous protomer to purified TTSSs (*S. typhimurium* with MxiH* and *S. flexneri* with PrgI*, data not shown). Consistently, *S. typhimurium* or *S. flexneri*, which were genetically complemented with the heterologous protomer, did not form needles and were unable to restore host invasion[23]. These experiments suggest that there is a structural incompatibility of needle proteins and TTSSs from different bacteria, in agreement with electrostatic differences in protomer surfaces found by previous work[23].

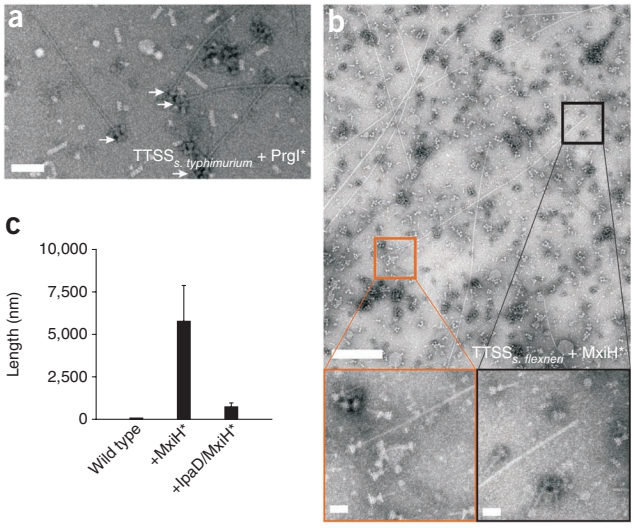

We tested the *in vitro* needle elongation by adding capping proteins such as IpaD, which forms the tip of the TTSS in *S. flexneri*[13,15]. We reasoned that, if needle elongation reflected a physiological process, the addition of these capping proteins should arrest needle growth. Indeed, whereas incubation of TTSS isolated from *S. flexneri* with MxiH* yielded an average needle length of 5 µm, TTSS incubated with both MxiH* and IpaD had an average needle length of 1 µm (**Fig. 2c**).

Isolated TTSS was most likely to grow in the absence of ATP or any other energy source, indicating that secreted PrgI* and MxiH* assemble spontaneously at the distal end. Therefore, it is likely that the unfolding in the cytoplasm and transport of the protomer through the needle require energy *in vivo*[24], but the assembly does not. Taken together, these *in vitro* experiments examining needle elongation support the model of a distal addition of the protomer to the needle and are consistent with reports showing that the structurally related flagellum is also elongated at the distal end[22].

X-ray crystal and solution-state NMR structure of PrgI*

To further understand the polymerization of the protomer during needle formation, we analyzed the structure of PrgI* in solution and in needles. Purified PrgI* is predominantly α-helical and monomeric in solution, as proven by circular dichroism and analytical ultracentrifugation (**Supplementary Fig. 5**). X-ray crystallography showed that residues starting from Gly19 to the C terminus of PrgI* adopt an α-helical hairpin conformation (**Fig. 3a** and **Table 1**). ESI-MS showed that crystallized PrgI* was not proteolytically degraded, indicating multiple conformations of the N-terminal 18 residues in the crystal. The ensemble of 25 NMR solution structures (**Table 2**, **Supplementary Fig. 6a**, representative NMR structure in **Fig. 3a** and HSQC spectrum in **Supplementary Fig. 7**) show a defined N terminus of the protomer, resulting in structural information for residues Trp5–Arg80 (r.m.s. deviation of 0.56 Å for Cα atoms). In solution, the NMR parameters indicate a helical conformation for residues

Figure 2 *In vitro* assembly of TTSS needles. (**a**) Purified PrgI* was incubated with isolated TTSS (arrow) from *S. typhimurium* and analyzed by TEM (scale bar, 0.1 µm). (**b**) TTSS from an *S. flexneri* strain were incubated with purified MxiH* and visualized (scale bar, 1 µm). Lower images show enlarged regions (scale bar, 0.1 µm). (**c**) Length of needles of isolated TTSS from *S. flexneri* without addition of purified protomer and of elongated needles obtained after incubation of TTSS from *S. flexneri* with purified MxiH* or purified IpaD and MxiH*. Error bars, s.d. ($n = 20$).

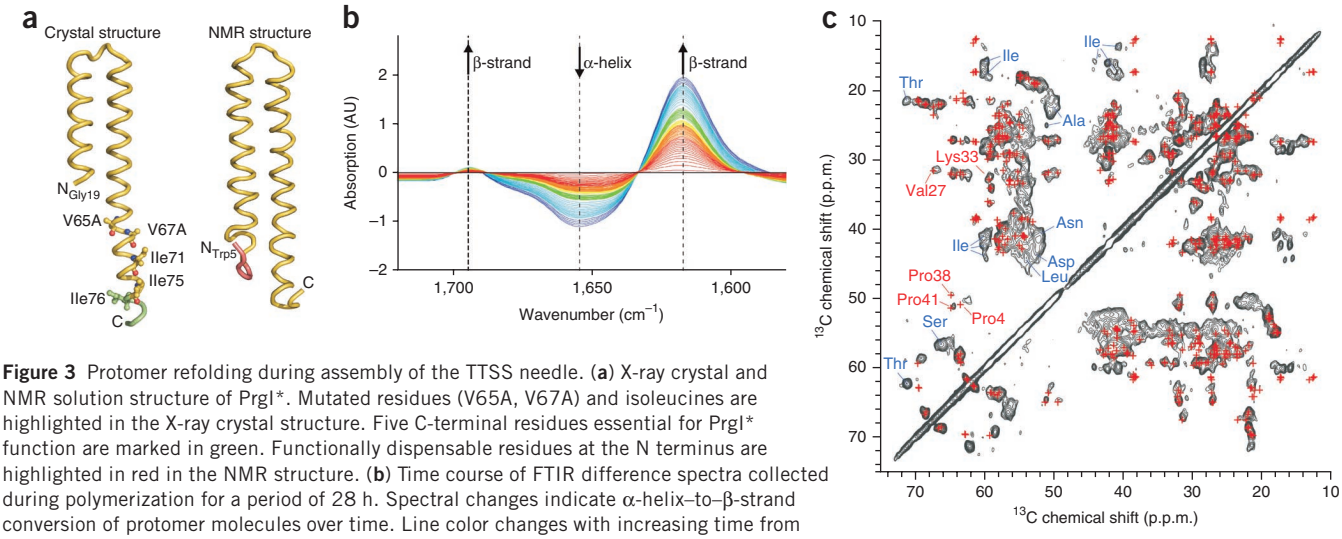

Figure 3 Protomer refolding during assembly of the TTSS needle. (**a**) X-ray crystal and NMR solution structure of PrgI*. Mutated residues (V65A, V67A) and isoleucines are highlighted in the X-ray crystal structure. Five C-terminal residues essential for PrgI* function are marked in green. Functionally dispensable residues at the N terminus are highlighted in red in the NMR structure. (**b**) Time course of FTIR difference spectra collected during polymerization for a period of 28 h. Spectral changes indicate α-helix–to–β-strand conversion of protomer molecules over time. Line color changes with increasing time from red to purple. (**c**) Solid-state NMR (^{13}C,^{13}C) correlation spectrum of PrgI* in needles (black contours) in comparison with chemical-shift correlations corresponding to solution-state NMR assignments (red crosses). Correlations labeled with blue residue codes are unique to solid-state spectra and correspond to β-strand backbone structure.

Asp11–Thr18, showing an extension of the N-terminal helix compared to that of the crystal structure. The core regions (residues Gly19–Lys37 and Ala42–Tyr57) of the NMR and X-ray structures superimpose well (**Supplementary Fig. 6b**), with an r.m.s. deviation of 0.77 Å for Cα atoms. The two structures show slightly different helical conformations at the C terminus, which might be explained by crystal packing. Notably, chemical-shift deviations from random coil values (secondary chemical shifts) for Cα nuclei of PrgI* suggest a reduced α-helix propensity outside of the core region defined above (**Supplementary Fig. 8**). These deviations can be explained by a higher flexibility of residues Asp11–Thr18 in the N-terminal α-helix and Gln61–Asn78 in the C-terminal α-helix of PrgI*. Overall, the structures indicate that the C terminus of PrgI* is α-helical, including the last five residues, and that the N terminus is flexible.

Mutational analysis shows that the six N-terminal residues of PrgI were dispensable for TTSS function, as determined by host-cell invasion (*prgI* plasmids (p*prgI*) p*prgI* ΔN6 and p*prgI* ΔN8 in **Fig. 1a**). In contrast, the C terminus of PrgI is required for needle formation and invasion (p*prgI* ΔC5 and p*prgI* ΔC-His in **Fig. 1a**), as already reported[23,25–28]. Previous structural studies of different TTSS needle protomers using NMR[23,27] or X-ray crystallography[29] were limited to C-terminal truncation mutants. These data show that the crystal and NMR structures presented here are the first ones[29,30] to our knowledge of a functional TTSS needle construct (PrgI*) before polymerization, as opposed to previous studies (**Supplementary Fig. 9**). This structure may reflect the conformation of the protomer in the cytosol.

PrgI* polymerization is coupled with a conformational change

To detect conformational changes in the protomer upon attachment to the needle, we recorded time-dependent Fourier transform infrared (FTIR) spectra of purified PrgI* (**Fig. 3b**). The α-helical character of the protomer before polymerization is shown by the amide-I band at 1,655 cm^{-1} (ref. 31) (downward arrow in **Fig. 3b**). The time-resolved difference spectra showed a decrease of the amide-I band intensity as well as two increasing bands indicative of β-strand formation at 1,617 cm^{-1} and 1,694 cm^{-1} (upward arrows in **Fig. 3b**). Thus, a backbone α-helix–to–β-strand conversion[31] in PrgI* affecting ~20% of the residues occurs simultaneously with the polymerization process (see **Supplementary Methods**).

C terminus of polymerized PrgI* adopts β-strand conformation

To locate the residues involved in the α-helix–to–β-strand conversion, the structure of PrgI* within the needle was probed with magic-angle spinning (MAS) solid-state NMR spectroscopy (ssNMR). Multidimensional correlation spectra confirmed α-helical and random-coil secondary structure, in line with a helical core and flexible termini. Notably, ssNMR spectra, in agreement with FTIR data from the needle, indicate protomer regions in a β-strand conformation. At the least, these conformations relate to

Table 1 Data collection and refinement statistics (molecular replacement)

	PrgI*
Data collection	
Space group	$P3_112$
Cell dimensions	
a, *c* (Å)	64.53, 104.29
Resolution (Å)	50.00–2.25 (2.31–2.25)[a]
R_{merge}	0.11 (0.92)
$I / \sigma I$	9.83 (2.11)
Completeness (%)	94.9 (96.8)
Redundancy	7.5 (7.6)
Refinement	
Resolution (Å)	38.13–2.45
No. reflections	8,544
R_{work} / R_{free}	0.225 / 0.239
No. atoms	
Protein	958
Water	9
B-factors	
Protein	81.64
Water	76.19
R.m.s. deviations	
Bond lengths (Å)	0.008
Bond angles (°)	1.1

One crystal was used.
[a]Values in parentheses are for highest-resolution shell.

Table 2 NMR and refinement statistics for monomeric PrgI*

	PrgI*
NMR distance and dihedral constraints	
Distance constraints	
Total NOE	837
Intra-residue	262
Inter-residue	575
Sequential ($\|i-j\|=1$)	299
Medium-range ($\|i-j\|<4$)	188
Long-range ($\|i-j\|>5$)	88
Intermolecular	–
Hydrogen bonds	–
Total dihedral angle restraints	374
ϕ	131
ψ	98
Total RDCs	36
Structure statistics	
Violations (mean ± s.d.)	
Distance constraints (Å)	0.03 ± 0.001
Dihedral angle constraints (°)	0.42 ± 0.035
Max. dihedral angle violation (°)	4.04
Max. distance constraint violation (Å)	0.40
Deviations from idealized geometry	
Bond lengths (Å)	0.01
Bond angles (°)	0.65
Impropers (°)	0.52
Average pairwise r.m.s. deviation[a] (Å)	
Heavy	0.83 ± 0.11
Backbone	0.36 ± 0.14

[a]r.m.s. deviation was calculated among 25 refined structures.

residue types alanine, aspartate, isoleucine, leucine, asparagine, serine and threonine (**Fig. 3c**, blue labels). In particular, the isoleucines, which are found within C-terminal residues 71–76 (**Fig. 3a**) exclusively, show only β-strand chemical shifts after needle formation. Except for the described β-strand correlations, we found an excellent match between solution- and solid-state NMR results (**Fig. 3c**). A list of possible backbone configurations for all residues in PrgI* is presented in **Supplementary Table 1** and **Supplementary Figure 10**.

Multiple unambiguous sequential resonance assignments, derived as shown in **Supplementary Figure 11** and denoted along the sequence in **Figure 4a**, further facilitated the localization of secondary-structure elements. The results point to two β-strands that comprise at least residues Ser62–Ala65 and Ile71–Ile76. Both β-strands potentially form a hairpin motif involving Lys69 and Asp70 (**Fig. 4a**,**b**), where Phe68 would account for the extended-strand phenylalanine resonances (**Supplementary Fig. 12**). The central helix-turn-helix motif comprising residues Val20–Glu53 is conserved, and possible extension by several residues in both directions is consistent with the spectra (**Fig. 3c**). In particular, both glutamates (Glu29 and Glu53) should reside within α-helices, as chemical-shift correlations for other secondary-structure elements are absent (**Supplementary Fig. 12**). Although random coil–type chemical shifts from solution for N-terminal residues match well with the ssNMR spectra, a detailed structural description for this segment remains elusive. Notably, chemical shifts for Thr18 and Gly19 suggest a stabilization of the α-helix for these two residues relative to solution. We probed a potential β-sheet comprising Tyr8 and Leu9 with C-terminal residues, which would be compatible with several unassigned tyrosine and leucine correlations, by comparing spectra for PrgI* with and without additional Y8A and L9A mutations. Based on the high similarity of the spectra, we ruled out this possibility (**Supplementary Fig. 13**). Furthermore, the presence of a leucine spin system in INEPT-based spectra that contain only signals from flexible protein segments (**Supplementary Fig. 14**) supports that the N terminus is indeed disordered at least up to residue Leu9. We detected multiple signal sets, which may be attributed to polymorphism, for threonine and isoleucine, and likewise, spectral overlap could be aggravated for other residues. PrgI* chemical-shift characteristics were reproduced over all four uniformly labeled samples used in total. In summary, the soluble protomer adopts an α-helical hairpin structure that, during needle assembly, changes conformation into two extended strands comprising approximately the C-terminal 18 residues of PrgI*.

It is noteworthy that mutated residues V65A and potentially V67A as well as wild-type residue Ile76 at the C terminus, which was deleted in mutants used in previous studies, are part of the β-strand in protomer needles. As the β-sheet propensity of valine is higher than that of alanine, it is likely that the α-helix–to–β-strand transformation accounts for the formation of the needle. Due to the high sequence similarity of the protomers[10] (**Supplementary Fig. 1**), we expect that the C-terminal β-sheet is essential for the TTSS needle assembly in various different bacterial pathogens.

DISCUSSION

In summary, we developed a functional and soluble protomer mutant, which allowed us to detect important steps in the assembly of TTSS needles. The needle protomer adopts an α-helical hairpin-like structure before polymerization. This may reflect the protein conformation inside the bacterial cytosol (**Figs. 3a** and **4a**,**b**, state I), which, for some protomer homologs, might be trapped by binding specific chaperones[19,32–34]. As shown by previous work, the protomer is mounted by the annular portion of the TTSS in a process that involves proteins like PrgJ in *S. typhimurium* forming the central rod of this protein complex[20]. Notably, we found that the TTSS needle itself serves as a polymerization nucleus for the ATP-independent addition of protomers (**Fig. 2**). Hence, after the first protomer molecules are positioned by additional 'scaffolding' proteins[8,18,20], the needle may provide a polymerization platform for arriving protomer molecules. In living bacteria, protomer molecules are unfolded in an energy-dependent process and may be transported[24,35,36] through the channel formed by the TTSS toward the distal end of the growing needle (**Fig. 4b**). In *S. flexneri*, the inner needle diameter was determined to be 20–30 Å in size. This channel diameter would allow the passage of a folded helix, or even a helical hairpin, through the TTSS. The spontaneous polymerization (**Fig. 3a**,**b**) of protomer into TTSS needles requires a conformational change in the C-terminal helix of the protein into a β-sheet conformation

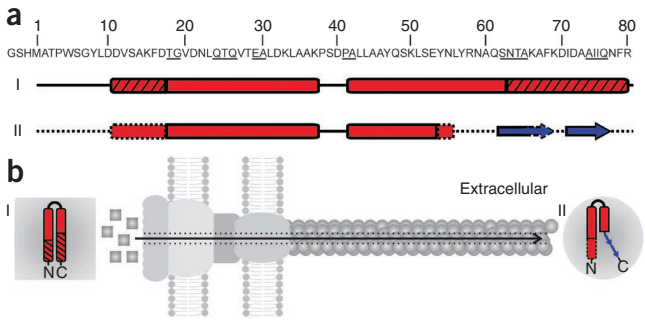

Figure 4 Assembly of the TTSS needle. (**a**) Proposed secondary structure of PrgI* before (stage I) polymerization and after (stage II) forming needles (α-helix, bar; β-strand, arrow; random coil, line). Hatched regions in stage I correspond to secondary structure with higher flexibility. For dashed regions in stage II, no unambiguous resonance assignments are available. (**b**) Model of needle constitution. Cytosolic protomer is transported by the TTSS to the tip of the growing needle.

(**Fig. 4a**,**b**, state II). It is noteworthy to compare the assembly of the TTSS and the flagellum, which are closely related. It is not known whether protomer refolding is required for the assembly of the flagellum[35]. As the flagellum also grows at the tip, it will be rewarding to determine whether the structural changes observed here are unique to the TTSS.

The observed conformational changes of the protomer from α-helix to partially β-sheet are fundamental for a correct description of the TTSS needle structure in the future. Structure determination of the protomer in the needle at atomic resolution using solid-state NMR is currently in progress in our laboratories. Because assembly of the TTSS needle is essential for bacterial virulence, searching for substances that inhibit protomer refolding could lead to the discovery of a novel target for the development of compounds that specifically interfere with pathogenic enterobacteria.

METHODS

Methods and any associated references are available in the online version of the paper at http://www.nature.com/nsmb/.

Accession codes. Protein Data Bank: Coordinates for PrgI* obtained by X-ray crystallography and solution-state NMR have been deposited with accession codes 2X9C and 2KV7, respectively.

Note: Supplementary information is available on the Nature Structural & Molecular Biology website.

ACKNOWLEDGMENTS

We thank P. Jungblut and M. Schmid for help with MS analysis, V. Brinkmann and U. Abu Abed for help with electron microscopy sample preparation, U. Müller and S. Monaco for assistance in using beamlines, M. Luft for providing the opportunity of the FTIR measurements and for helpful discussions, B. Angerstein for help with ssNMR sample preparation, D. Lee for help in using Bruker spectrometers and B. Raupach, A. Zumsteg, F. Meissner, M. Lunelli and R. Kumar Lokareddy for their useful comments and critical reading of the manuscript. This work was supported by the Max-Planck-Society (to C. Griesinger and A.Z.) and by the Deutsche Forschungsgemeinschaft through an Emmy Noether stipend (LA 2705/1-1) to A.L.

AUTHOR CONTRIBUTIONS

Ö.P. cloned constructs and purified protomer for every experiment, crystallized, collected, processed and refined X-ray diffraction data and performed cellular assays; H.S. collected, processed and analyzed liquid-state NMR data and performed FTIR experiments and ThioflavinT binding assays; F.D. performed and analyzed DLS and X-ray fiber diffraction experiments; K.S. and C.A. collected, processed and analyzed solid-state NMR data; H.T. and Ö.P. purified and performed *in vitro* growth experiments with TTSS; C. Goosmann performed TEM studies; A.L. and M.B. designed and analyzed solid-state NMR experiments; C. Griesinger designed and analyzed liquid-state NMR experiments; A.T. designed and analyzed DLS and X-ray fiber diffraction experiments; V.B. designed TEM experiments; A.Z. designed functional and structural experiments; M.K. conceived this study, designed functional and TEM experiments, collected, refined and analyzed X-ray diffraction data and wrote the paper; all authors discussed the results and commented on the manuscript.

COMPETING FINANCIAL INTERESTS

The authors declare no competing financial interests.

Published online at http://www.nature.com/nsmb/.
Reprints and permissions information is available online at http://npg.nature.com/reprintsandpermissions/.

1. Kubori, T. *et al.* Supramolecular structure of the *Salmonella typhimurium* type III protein secretion system. *Science* **280**, 602–605 (1998).
2. Journet, L., Agrain, C., Broz, P. & Cornelis, G.R. The needle length of bacterial injectisomes is determined by a molecular ruler. *Science* **302**, 1757–1760 (2003).
3. Tamano, K. *et al.* Supramolecular structure of the *Shigella* type III secretion machinery: the needle part is changeable in length and essential for delivery of effectors. *EMBO J.* **19**, 3876–3887 (2000).
4. Cornelis, G.R. The type III secretion injectisome. *Nat. Rev. Microbiol.* **4**, 811–825 (2006).
5. Galan, J.E. & Wolf-Watz, H. Protein delivery into eukaryotic cells by type III secretion machines. *Nature* **444**, 567–573 (2006).
6. Nhieu, G.T. & Sansonetti, P.J. Mechanism of *Shigella* entry into epithelial cells. *Curr. Opin. Microbiol.* **2**, 51–55 (1999).
7. Kimbrough, T.G. & Miller, S.I. Assembly of the type III secretion needle complex of *Salmonella typhimurium*. *Microbes Infect.* **4**, 75–82 (2002).
8. Marlovits, T.C. *et al.* Structural insights into the assembly of the type III secretion needle complex. *Science* **306**, 1040–1042 (2004).
9. Blocker, A. *et al.* Structure and composition of the *Shigella flexneri* 'needle complex', a part of its type III secreton. *Mol. Microbiol.* **39**, 652–663 (2001).
10. Blocker, A.J. *et al.* What's the point of the type III secretion system needle? *Proc. Natl. Acad. Sci. USA* **105**, 6507–6513 (2008).
11. Kawagishi, I., Homma, M., Williams, A.W. & Macnab, R.M. Characterization of the flagellar hook length control protein fliK of *Salmonella typhimurium* and *Escherichichia coli*. *J. Bacteriol.* **178**, 2954–2959 (1996).
12. Espina, M. *et al.* IpaD localizes to the tip of the type III secretion system needle of *Shigella flexneri*. *Infect. Immun.* **74**, 4391–4400 (2006).
13. Mota, L.J. Type III secretion gets an LcrV tip. *Trends Microbiol.* **14**, 197–200 (2006).
14. Mueller, C.A. *et al.* The V-antigen of *Yersinia* forms a distinct structure at the tip of injectisome needles. *Science* **310**, 674–676 (2005).
15. Sani, M. *et al.* IpaD is localized at the tip of the *Shigella flexneri* type III secretion apparatus. *Biochim. Biophys. Acta* **1770**, 307–311 (2007).
16. Rogers, D.R. Screening for amyloid with the thioflavin-T fluorescent method. *Am. J. Clin. Pathol.* **44**, 59–61 (1965).
17. Blake, C.C.F. *et al. Nature and Origin of Amyloid Fibrils*. CIBA Foundation Symposium, No. 199 (1996).
18. Cordes, F.S. *et al.* Helical structure of the needle of the type III secretion system of *Shigella flexneri*. *J. Biol. Chem.* **278**, 17103–17107 (2003).
19. Quinaud, M. *et al.* The PscE-PscF-PscG complex controls type III secretion needle biogenesis in *Pseudomonas aeruginosa*. *J. Biol. Chem.* **280**, 36293–36300 (2005).
20. Marlovits, T.C. *et al.* Assembly of the inner rod determines needle length in the type III secretion injectisome. *Nature* **441**, 637–640 (2006).
21. Bishop, M.F. & Ferrone, F.A. Kinetics of nucleation-controlled polymerization. A perturbation treatment for use with a secondary pathway. *Biophys. J.* **46**, 631–644 (1984).
22. Emerson, S.U., Tokuyasu, K. & Simon, M.I. Bacterial flagella: polarity of elongation. *Science* **169**, 190–192 (1970).
23. Wang, Y. *et al.* Differences in the electrostatic surfaces of the type III secretion needle proteins PrgI, BsaL, and MxiH. *J. Mol. Biol.* **371**, 1304–1314 (2007).
24. Akeda, Y. & Galan, J.E. Chaperone release and unfolding of substrates in type III secretion. *Nature* **437**, 911–915 (2005).
25. Darboe, N., Kenjale, R., Picking, W.L., Picking, W.D. & Middaugh, C.R. Chemical denaturation of MxiH from *Shigella* and PrgI from *Salmonella*. *Protein Sci.* **15**, 543–552 (2006).
26. Deane, J.E. *et al.* Expression, purification, crystallization and preliminary crystallographic analysis of MxiH, a subunit of the *Shigella flexneri* type III secretion system needle. *Acta Crystallogr. F Struct. Biol. Cryst. Commun.* **62**, 302–305 (2006).
27. Zhang, L., Wang, Y., Picking, W.L., Picking, W.D. & De Guzman, R.N. Solution structure of monomeric BsaL, the type III secretion needle protein of *Burkholderia pseudomallei*. *J. Mol. Biol.* **359**, 322–330 (2006).
28. Barrett, B.S., Picking, W.L., Picking, W.D. & Middaugh, C.R. The response of type three secretion system needle proteins MxiHDelta5, BsaLDelta5, and PrgIDelta5 to temperature and pH. *Proteins* **73**, 632–643 (2008).
29. Deane, J.E. *et al.* Molecular model of a type III secretion system needle: implications for host-cell sensing. *Proc. Natl. Acad. Sci. USA* **103**, 12529–12533 (2006).
30. Kenjale, R. *et al.* The needle component of the type III secreton of *Shigella* regulates the activity of the secretion apparatus. *J. Biol. Chem.* **280**, 42929–42937 (2005).
31. Oberg, K.A., Ruysschaert, J.M. & Goormaghtigh, E. Rationally selected basis proteins: a new approach to selecting proteins for spectroscopic secondary structure analysis. *Protein Sci.* **12**, 2015–2031 (2003).
32. Quinaud, M. *et al.* Structure of the heterotrimeric complex that regulates type III secretion needle formation. *Proc. Natl. Acad. Sci. USA* **104**, 7803–7808 (2007).
33. Sun, P., Tropea, J.E., Austin, B.P., Cherry, S. & Waugh, D.S. Structural characterization of the *Yersinia pestis* type III secretion system needle protein YscF in complex with its heterodimeric chaperone YscE/YscG. *J. Mol. Biol.* **377**, 819–830 (2008).
34. Tan, Y.W., Yu, H.B., Leung, K.Y., Sivaraman, J. & Mok, Y.K. Structure of AscE and induced burial regions in AscE and AscG upon formation of the chaperone needle-subunit complex of type III secretion system in *Aeromonas hydrophila*. *Protein Sci.* **17**, 1748–1760 (2008).
35. Minamino, T. & Namba, K. Distinct roles of the FliI ATPase and proton motive force in bacterial flagellar protein export. *Nature* **451**, 485–488 (2008).
36. Paul, K., Erhardt, M., Hirano, T., Blair, D.F. & Hughes, K.T. Energy source of flagellar type III secretion. *Nature* **451**, 489–492 (2008).

ONLINE METHODS

Cloning, gene expression and protein purification. *prgI* and *mxiH* were amplified from *S. enterica* serovar *typhimurium* strain SL1344 or *S. flexneri* strain M90T, respectively, by standard PCR using oligonucleotide primers with NdeI and XhoI restriction sites at either ends. PCR products were cloned into the expression vector pET-28a(+) (Novagen) containing an N-terminal histidine tag. For functional assays, *prgI* and *mxiH* were cloned into the pASK-IBA33(+) vector (IBA) as BsaI fragments. N- and C-terminal deletions as well as alanine point mutants were generated using the QuikChange Site-Directed Mutagenesis Kit (Stratagene). All constructs were confirmed by sequencing. Protomer mutants were expressed in *E. coli* BL21(DE3) RIL cells harboring the gene in pET-28a(+) expression vector. Cells were induced with isopropyl-β-D-1-thiogalactopyranoside and harvested after 4 h, and histidine-tagged protein was purified using affinity chromatography (HisTrap, GE Healthcare). Bound protein was washed (80 mM imidazole) and eluted using buffer containing 500 mM imidazole. After buffer exchange (20 mM HEPES, pH 7.4, 50 mM NaCl), the tag was cleaved with the CleanCleave Kit (Sigma-Aldrich). The cleaved product was purified by size-exclusion chromatography (Superdex 200, GE Healthcare) and stored at 4 °C until use. For ^{15}N and/or ^{13}C labeling of PrgI*, M9 minimal medium was complemented with [^{15}N]–ammonium chloride and [$^{13}C_6$]-glucose.

Crystallization, data collection, structure determination and refinement. Hexagonal crystals of PrgI* were obtained at 18 °C using hanging-drop vapor diffusion technique mixing equal volumes of protein and reservoir solution containing 150 mM $NH_4H_2PO_4$. Crystals of space group *P*312 ($a = b = 64.53$ Å, $c = 104.29$ Å, $\alpha = \beta = 90°$, $\gamma = 120°$) containing two copies of the protein per asymmetric unit were flash frozen in liquid nitrogen in the presence of 30% (v/v) glycerol. X-ray diffraction data were collected at 100 K and at a wavelength of 0.97625 Å at the European Synchrotron Radiation Facility (ID 23-1). Data were indexed, integrated and scaled using the program package XDS[37] and analyzed for merohedral twinning using the Padilla-Yeates Algorithm[38] and CNS[39]. The crystal structure of PrgI* was solved by molecular replacement with Phaser[40] using MxiH (PDB 2CA5) as a template. The initial model was refined by repeated cycles of manual building and refinement using the programs Coot[41] and CNS[39]. Ramachandran analysis[42] of the X-ray crystal structure of PrgI* showed that 96.5% of the residues were in their most favored conformations, and the other 3.5% were in allowed conformations.

Generation of knockout strains. Bacterial knockouts were generated according to previous work[43]. pASK-IBA(+) plasmids harboring wild-type or mutant *prgI* (p*prgI*) or *mxiH* (p*mxiH*) were used to complement deletions of *prgI* in *S. typhimurium* strain SL1344 and *mxiH* in *S. flexneri* to generate strains SL1344 Δ*prgI*/p*prgI* and M90T Δ*mxiH*/p*mxiH*, respectively.

HeLa cell invasion assay. HeLa cells were seeded at 1×10^5 cells per well and grown for 24 h at 37 °C. Prior to infection, growth medium was aspirated, cells were washed twice with PBS and serum-free medium was added. To test for epithelial cell invasion and intracellular growth, HeLa cells were infected with *S. typhimurium* at a multiplicity of infection of 10:1. Expression of *prgI* and *mxiH* was induced with 0.2 μg ml^{-1} anhydrotetracycline for 1 h. Bacterial inocula were prepared in PBS and centrifuged onto cells (700*g*, 10 min), and infected cultures were incubated for 20 min at 37 °C. Cultures were washed three times with PBS, and fresh medium containing 100 μg ml^{-1} gentamicin was added. After 2 h, cells were washed with PBS and lysed with 0.1% (w/v) Triton X-100. Numbers of viable bacteria were obtained by plating dilutions of lysates on tryptic soy agar plates and counting colonies after overnight (16 h) incubation at 37 °C.

Isolation of the needle complex. Needle complex from *S. typhimurium* or *S. flexneri* was extracted and purified according to a modified protocol described previously[44] (Xiang *et al.*, personal communication). Each needle complex consists of a membrane-embedded base and an extracellular needle-shaped structure with a typical length of 50–70 nm.

Analytical ultracentrifugation. Analytical ultracentrifugation sedimentation velocity experiments were performed in an XL-I Analytical Ultracentrifuge (BeckmanCoulter) using the interference optics of the instrument. Freshly purified PrgI* (1.0 mg ml^{-1}) was measured at 4 °C and 116,480*g* (BeckmanCoulter An-50Ti rotor) in the presence of 20 mM HEPES, pH 7.5, 50 mM NaCl (Nanolytics). Data were analyzed with the program NONLIN (http://www.biotech.uconn.edu/auf/?i=aufftp).

Solution-state NMR data acquisition and processing. NMR spectra were acquired at 14.1, 18.8 and 21.1 T on Bruker Avance spectrometers (Bruker AG, Karlsruhe, Germany) at 283 K with samples containing ~0.3 mM PrgI* in 20 mM MES, pH 5.5, and 20 mM NaCl buffer in the presence of 93% (v/v) H_2O/7% (v/v) ^2H_2O. Freshly purified protein at low concentration (0.3 mM) was used to delay polymerization. Spectral patterns did not change during the acquisition of NMR spectra. The anisotropic sample for extraction of 36 RDCs was prepared by addition of 18 mg ml^{-1} pf1 phages as alignment medium to the NMR sample. Data were processed with NMRPipe[45] and analyzed with CARA[46]. Ramachandran analysis of the NMR structure of PrgI* showed that 84.2% of the residues were in their most favored conformations, and the other 15.8% were in allowed conformations.

Sequential/side chain assignment. Sequential assignments of PrgI* were accomplished by a combination of (^1H-^{15}N)-HSQC[47,48], (^1H-^{13}C)-HSQC[49], HNCACB[50], HNCA[51], CBCA(CO)NH[52], HNCO[53], (H)CCH-COSY and (H)CCH-TOCSY[54]. Aromatic resonance assignments were made using the (^1H-^1H-^{15}N) and (^1H-^1H-^{13}C) 3D NOESY spectra. (^1H-^{15}N)-RDCs were determined from resonance splitting in (^1H-^{15}N) TROSY-HSQC[55] and (^1H-^{15}N) COCAINE spectra[56] (modified version) in isotropic and anisotropic samples.

Electron microscopy. Sample solutions were applied to glow-discharged carbon-coated copper grids, incubated for 2 min, washed and contrasted with 4% (w/v) PTA for 1 min. Specimens were examined with a Leo912 AB (Zeiss SMT) transmission electron microscope equipped with a side-mounted Cantega digital camera (Olympus SIS).

Dynamic light scattering. Measurements were carried out using a Malvern Instruments particle sizer (Zetasizer Nano ZS, Malvern Instruments) equipped with a He-Ne laser ($\lambda = 632.8$ nm). DLS was performed at 25 °C in backscattering modus at a scattering angle of $2\theta = 173°$ with 10 mm × 10 mm quartz cuvettes. Prior to measurement, the sample was filtered with a 0.45-μm syringe filter (Millipore). The Stokes-Einstein relation was used to calculate the hydrodynamic radius (Malvern Dispersion Technology Software 5.02).

Solid-state NMR. Multidimensional solid-state NMR correlation spectra[57,58] were recorded at 18.8 and 20.0 T with Bruker Avance II/III spectrometers using 10–15 mg PrgI* (see **Supplementary Methods** for details).

37. Kabsch, W. Automatic processing of rotation diffraction data from crystals of initially unknown symmetry and cell constants. *J. Appl. Crystallogr.* **26**, 795–800 (1993).
38. Padilla, J.E. & Yeates, T.O. A statistic for local intensity differences: robustness to anisotropy and pseudo-centering and utility for detecting twinning. *Acta Crystallogr. D Biol. Crystallogr.* **59**, 1124–1130 (2003).
39. Brunger, A.T. *et al.* Crystallography & NMR system: A new software suite for macromolecular structure determination. *Acta Crystallogr. D Biol. Crystallogr.* **54**, 905–921 (1998).
40. McCoy, A.J. *et al.* Phaser crystallographic software. *J. Appl. Crystallogr.* **40**, 658–674 (2007).
41. Emsley, P. & Cowtan, K. Coot: model-building tools for molecular graphics. *Acta Crystallogr. D Biol. Crystallogr.* **60**, 2126–2132 (2004).
42. Laskowski, R.A., MacArthur, M.W., Moss, D.S. & Thornton, J.M. PROCHECK—a program to check the stereochemical quality of protein structures. *J. Appl. Crystallogr.* **26**, 283–291 (1993).
43. Datsenko, K.A. & Wanner, B.L. One-step inactivation of chromosomal genes in *Escherichia coli* K-12 using PCR products. *Proc. Natl. Acad. Sci. USA* **97**, 6640–6645 (2000).
44. Kubori, T. *et al.* Supramolecular structure of the *Salmonella typhimurium* type III protein secretion system. *Science* **280**, 602–605 (1998).
45. Delaglio, F. *et al.* NMRPipe: A multidimensional spectral processing system based on UNIX pipes. *J. Biomol. NMR* **6**, 277–293 (1995).
46. Keller, R. *The Computer Aided Resonance Assignment Tutorial* 1st edn. (CANTINA Verlag, Goldau, Switzerland, 2004).
47. Bodenhausen, G. & Ruben, D.J. Natural abundance nitrogen-15 NMR by enhanced heteronuclear spectroscopy. *Chem. Phys. Lett.* **69**, 185–189 (1980).
48. Grzesiek, S. & Bax, A. Amino acid type determination in the sequential assignment procedure of uniformly $^{13}C/^{15}N$-enriched proteins. *J. Biomol. NMR* **3**, 185–204 (1993).

49. Kay, L.E., Keifer, P. & Saarinen, T. Pure absorption gradient enhanced heteronuclear single quantum correlation spectroscopy with improved sensitivity. *J. Am. Chem. Soc.* **114**, 10663–10665 (1992).
50. Wittekind, M. & Mueller, L. HNCACB, a high-sensitivity 3D NMR experiment to correlate amide-proton and nitrogen resonances with the α- and β-carbon resonances in proteins. *J. Magn. Reson. B* **101**, 201–205 (1993).
51. Bax, A. & Ikura, M. An efficient 3D NMR technique for correlating the proton and ^{15}N backbone amide resonances with the α-carbon of the preceding residue in uniformly ^{15}N/^{13}C enriched proteins. *J. Biomol. NMR* **1**, 99–104 (1991).
52. Grzesiek, S. *et al.* Proton, carbon-13, and nitrogen-15 NMR backbone assignments and secondary structure of human interferon-γ. *Biochemistry* **31**, 8180–8190 (1992).
53. Ikura, M., Kay, L.E. & Bax, A. A novel approach for sequential assignment of proton, carbon-13, and nitrogen-15 spectra of larger proteins: heteronuclear triple-resonance three-dimensional NMR spectroscopy. Application to calmodulin. *Biochemistry* **29**, 4659–4667 (1990).
54. Bax, A., Clore, G.M. & Gronenborn, A.M. ^{1}H-^{1}H correlation via isotropic mixing of carbon-13 magnetization, a new three-dimensional approach for assigning proton and carbon-13 spectra of carbon-13-enriched proteins. *J. Magn. Reson.* **88**, 425–431 (1990).
55. Pervushin, K., Riek, R., Wider, G. & Wuthrich, K. Attenuated T-2 relaxation by mutual cancellation of dipole-dipole coupling and chemical shift anisotropy indicates an avenue to NMR structures of very large biological macromolecules in solution. *Proc. Natl. Acad. Sci. USA* **94**, 12366–12371 (1997).
56. Lee, D., Vogeli, B. & Pervushin, K. Detection of C′,Cα correlations in proteins using a new time- and sensitivity-optimal experiment. *J. Biomol. NMR* **31**, 273–278 (2005).
57. Baldus, M. Molecular Interactions investigated by multi-dimensional solid-state NMR. *Curr. Opin. Struct. Biol.* **16**, 618–623 (2006).
58. Seidel, K. *et al.* Protein solid-state NMR resonance assignments from (^{13}C,^{13}C) correlation spectroscopy. *Phys. Chem. Chem. Phys.* **6**, 5090–5093 (2004).

doi:10.1038/nsmb.1822